Research Article | Vol. 25, No. 5 | 6 Mar 2017 | OPTICS EXPRESS 5255

Optics EXPRESS

Strong plasmonic confinement and optical force in phosphorene pairs

HUA LU,[1,2,4] YONGKANG GONG,[3] DONG MAO,[1,2] XUETAO GAN,[1,2] AND JIANLIN ZHAO[1,2,5]

[1]*MOE Key Laboratory of Space Applied Physics and Chemistry, School of Science, Northwestern Polytechnical University, Xi'an 710072, China*
[2]*Shaanxi Key Laboratory of Optical Information Technology, School of Science, Northwestern Polytechnical University, Xi'an 710072, China*
[3]*Wireless and Optoelectronics Research and Innovation Centre (WORIC), Faculty of Computing, Engineering and Science, University of South Wales, Cardiff CF37 1DL, United Kingdom*
[4]*hualu@nwpu.edu.cn*
[5]*jlzhao@nwpu.edu.cn*

Abstract: The plasmonic responses in the spatially separated phosphorene (single-layer black phosphorus) pairs are investigated, mainly containing the field enhancement, light confinement, and optical force. It is found that the strong anisotropic dispersion of black phosphorus gives rise to the direction-dependent symmetric and anti-symmetric plasmonic modes. Our results demonstrate that the symmetrical modes possess stronger field enhancement, higher light confinement, and larger optical force than the anti-symmetric modes in the nanoscale structures. Especially, the light confinement ratio and optical force for the symmetric mode along the armchair direction of black phosphorus can reach as high as >90% and >3000 pN/mW, respectively. These results may open a new door for the light manipulation at nanoscale and the design of black phosphorus based photonic devices.

© 2017 Optical Society of America

OCIS codes: (240.6680) Surface plasmons; (310.6860) Thin films, optical properties.

References and links

1. W. L. Barnes, A. Dereux, and T. W. Ebbesen, "Surface plasmon subwavelength optics," Nature **424**(6950), 824–830 (2003).
2. D. Gramotnev, and S. Bozhevolnyi, "Plasmonics beyond the diffraction limit," Nat. Photonics **4**(2), 83–91 (2010).
3. R. F. Oulton, V. J. Sorger, T. Zentgraf, R. M. Ma, C. Gladden, L. Dai, G. Bartal, and X. Zhang, "Plasmon lasers at deep subwavelength scale," Nature **461**(7264), 629–632 (2009).
4. C. Genet, and T. W. Ebbesen, "Light in tiny holes," Nature **445**(7123), 39–46 (2007).
5. H. Lu, X. Liu, and D. Mao, "Plasmonic analog of electromagnetically induced transparency in multi-nanoresonator-coupled waveguide systems," Phys. Rev. A **85**(5), 053803 (2012).
6. B. Luk'yanchuk, N. I. Zheludev, S. A. Maier, N. J. Halas, P. Nordlander, H. Giessen, and C. T. Chong, "The Fano resonance in plasmonic nanostructures and metamaterials," Nat. Mater. **9**(9), 707–715 (2010).
7. H. Ren, X. Li, Q. Zhang, and M. Gu, "On-chip noninterference angular momentum multiplexing of broadband light," Science **352**(6287), 805–809 (2016).
8. C. Huang, and L. Zhu, "Enhanced optical forces in 2D hybrid and plasmonic waveguides," Opt. Lett. **35**(10), 1563–1565 (2010).
9. H. Lu, X. Liu, D. Mao, L. Wang, and Y. Gong, "Tunable band-pass plasmonic waveguide filters with nanodisk resonators," Opt. Express **18**(17), 17922–17927 (2010).
10. X. M. Goh, Y. Zheng, S. J. Tan, L. Zhang, K. Kumar, C. W. Qiu, and J. K. Yang, "Three-dimensional plasmonic stereoscopic prints in full colour," Nat. Commun. **5**, 5361 (2014).
11. H. Wei, Z. Wang, X. Tian, M. Käll, and H. Xu, "Cascaded logic gates in nanophotonic plasmon networks," Nat. Commun. **2**, 387 (2011).
12. K. S. Novoselov, A. K. Geim, S. V. Morozov, D. Jiang, Y. Zhang, S. V. Dubonos, I. V. Grigorieva, and A. A. Firsov, "Electric field effect in atomically thin carbon films," Science **306**(5696), 666–669 (2004).
13. M. Liu, X. Yin, E. Ulin-Avila, B. Geng, T. Zentgraf, L. Ju, F. Wang, and X. Zhang, "A graphene-based broadband optical modulator," Nature **474**(7349), 64–67 (2011).
14. H. Lu, X. Gan, B. Jia, D. Mao, and J. Zhao, "Tunable high-efficiency light absorption of monolayer graphene via Tamm plasmon polaritons," Opt. Lett. **41**(20), 4743–4746 (2016).

#284461 https://doi.org/10.1364/OE.25.005255
Journal © 2017 Received 11 Jan 2017; revised 21 Feb 2017; accepted 22 Feb 2017; published 27 Feb 2017

Optics EXPRESS

15. Q. Bao, H. Zhang, B. Wang, Z. Ni, C. Lim, Y. Wang, D. Tang, and K. Loh, "Broadband graphene polarizer," Nat. Photonics **5**(7), 411–415 (2011).
16. Z. Sun, T. Hasan, F. Torrisi, D. Popa, G. Privitera, F. Wang, F. Bonaccorso, D. M. Basko, and A. C. Ferrari, "Graphene mode-locked ultrafast laser," ACS Nano **4**(2), 803–810 (2010).
17. H. Lu, C. Zeng, Q. Zhang, X. Liu, M. M. Hossain, P. Reineck, and M. Gu, "Graphene-based active slow surface plasmon polaritons," Sci. Rep. **5**, 8443 (2015).
18. X. Gan, R. Shiue, Y. Gao, I. Meric, T. Heinz, K. Shepard, J. Hone, S. Assefa, and D. Englund, "Chip-integrated ultrafast graphene photodetector with high responsivity," Nat. Photonics **7**(11), 883–887 (2013).
19. L. Ju, B. Geng, J. Horng, C. Girit, M. Martin, Z. Hao, H. A. Bechtel, X. Liang, A. Zettl, Y. R. Shen, and F. Wang, "Graphene plasmonics for tunable terahertz metamaterials," Nat. Nanotechnol. **6**(10), 630–634 (2011).
20. A. Grigorenko, M. Polini, and K. Novoselov, "Graphene plasmonics," Nat. Photonics **6**(11), 749–758 (2012).
21. V. W. Brar, M. S. Jang, M. Sherrott, J. J. Lopez, and H. A. Atwater, "Highly confined tunable mid-infrared plasmonics in graphene nanoresonators," Nano Lett. **13**(6), 2541–2547 (2013).
22. H. Cheng, S. Chen, P. Yu, X. Duan, B. Xie, and J. Tian, "Dynamically tunable plasmonically induced transparency in periodically patterned graphene nanostrips," Appl. Phys. Lett. **103**(20), 203112 (2013).
23. Q. Zhang, X. Li, M. M. Hossain, Y. Xue, J. Zhang, J. Song, J. Liu, M. D. Turner, S. Fan, Q. Bao, and M. Gu, "Graphene surface plasmons at the near-infrared optical regime," Sci. Rep. **4**, 6559 (2014).
24. A. Vakil, and N. Engheta, "Transformation optics using graphene," Science **332**(6035), 1291–1294 (2011).
25. P. Alonso-González, A. Y. Nikitin, F. Golmar, A. Centeno, A. Pesquera, S. Vélez, J. Chen, G. Navickaite, F. Koppens, A. Zurutuza, F. Casanova, L. E. Hueso, and R. Hillenbrand, "Controlling graphene plasmons with resonant metal antennas and spatial conductivity patterns," Science **344**(6190), 1369–1373 (2014).
26. A. Yu. Nikitin, P. Alonso-González, and R. Hillenbrand, "Efficient coupling of light to graphene plasmons by compressing surface polaritons with tapered bulk materials," Nano Lett. **14**(5), 2896–2901 (2014).
27. P. Y. Chen, and A. Alù, "Atomically thin surface cloak using graphene monolayers," ACS Nano **5**(7), 5855–5863 (2011).
28. M. Engel, M. Steiner, and P. Avouris, "Black phosphorus photodetector for multispectral, high-resolution imaging," Nano Lett. **14**(11), 6414–6417 (2014).
29. L. Li, Y. Yu, G. J. Ye, Q. Ge, X. Ou, H. Wu, D. Feng, X. H. Chen, and Y. Zhang, "Black phosphorus field-effect transistors," Nat. Nanotechnol. **9**(5), 372–377 (2014).
30. S. Zhang, J. Yang, R. Xu, F. Wang, W. Li, M. Ghufran, Y. W. Zhang, Z. Yu, G. Zhang, Q. Qin, and Y. Lu, "Extraordinary photoluminescence and strong temperature/angle-dependent Raman responses in few-layer phosphorene," ACS Nano **8**(9), 9590–9596 (2014).
31. Z. Liu, and K. Aydin, "Localized surface plasmons in nanostructured monolayer black phosphorus," Nano Lett. **16**(6), 3457–3462 (2016).
32. J. Lu, J. Yang, A. Carvalho, H. Liu, Y. Lu, and C. H. Sow, "Light-matter interactions in phosphorene," Acc. Chem. Res. **49**(9), 1806–1815 (2016).
33. J. Yang, Z. Wang, F. Wang, R. Xu, J. Tao, S. Zhang, Q. Qin, B. Luther-Davies, C. Jagadish, Z. Yu, and Y. Lu, "Atomically thin optical lenses and gratings," Light Sci. Appl. **5**(3), e16046 (2016).
34. T. Low, R. Roldán, H. Wang, F. Xia, P. Avouris, L. M. Moreno, and F. Guinea, "Plasmons and screening in monolayer and multilayer black phosphorus," Phys. Rev. Lett. **113**(10), 106802 (2014).
35. Y. He, S. He, and X. Yang, "Optical field enhancement in nanoscale slot waveguides of hyperbolic metamaterials," Opt. Lett. **37**(14), 2907–2909 (2012).
36. Y. He, S. He, J. Gao, and X. Yang, "Giant transverse optical forces in nanoscale slot waveguides of hyperbolic metamaterials," Opt. Express **20**(20), 22372–22382 (2012).
37. X. Xu, L. Shi, Y. Liu, Z. Wang, and X. Zhang, "Enhanced optical gradient forces between coupled graphene sheets," Sci. Rep. **6**, 28568 (2016).
38. X. Yang, Y. Liu, R. F. Oulton, X. Yin, and X. Zhang, "Optical forces in hybrid plasmonic waveguides," Nano Lett. **11**(2), 321–328 (2011).

1. Introduction

Surface plasmon polaritons (SPPs) are electromagnetic waves travelling along dielectric-conductor interface and coupled to the free electron oscillations in the conductor [1, 2]. SPPs are considered as an excellent platform for realizing integrated photonic devices and manipulating light at nanoscale owing to their fantastic capacities of overcoming classical diffraction limit and confining light at deep subwavelength scale in visible and near-infrared ranges [2]. The unique behaviors of SPPs in metallic structures are also able to facilitate the development of highly integrated optical circuits [3]. So far, various significant optical phenomena have been found in the plasmonic systems, such as extraordinary optical transmission [4], electromagnetically induced transparency-like effect [5], Fano resonances [6], angular momentum multiplexing [7], and optical force [8]. Meanwhile, a large number of plasmonic components based on metallic structures have been proposed, including nanoscale lasers [3], filters [9], stereoscopic prints [10], logical gates [11], etc. The development of

Optics EXPRESS

novel optical materials plays a crucial role in promoting the revolution of optical technologies. Graphene, a two-dimensional (2D) single layer of carbon atoms, has exhibited outstanding features in electronics and optics after its successful exfoliation [12]. As a relatively new material, graphene injects enormous vitality for the realization of novel optical functions and excellent 2D photonic devices, such as electro-optical modulation [13], light absorption [14], optical polarization [15], mode-locking [16], slow light [17], photodetection [18], and so on. Recently, it was found that graphene could support the generation and propagation of SPPs in infrared and terahertz ranges [19–27]. Moreover, SPPs in 2D monolayer structures are regarded as an attractive tool for controlling light and enhancing light-matter interaction at nanoscale [27]. In particular, Plasmonics in the 2D material processes the strong field confinement and relatively low propagation loss, making the 2D material a promising one-atom-thick platform for light manipulation [17, 24]. Black phosphorus (BP), as a newly emerging 2D material, has attracted broad attention since it has the intrinsic band gap unlike graphene, providing great potential for optoelectronics [28–34]. In the single-layer BP (termed 'phosphorene'), phosphorous atoms covalently bonded with three others form a hexagonal lattice with a puckered honeycomb structure [29]. This special atomic structure gives rise to the highly anisotropic electron dispersion and direction-dependent conduction [30, 31]. The optoelectronic properties of BP were intensely investigated for applications in photodetection [28], field effect transistors [29], and light-matter interaction [32]. Lu *et al.* firstly reported atomically thin optical lenses and grating structure fabricated by the BP layers [33]. Quite recently, Low *et al.* theoretically proposed to excite SPPs in BP layer [34]. The localized surface plasmon resonance was numerically investigated in BP ribbon and patch arrays by Aydin *et al.* [31].

Exploring novel optical responses in BP nanostructures is of extreme importance to open the BP's broad applications in photonics and optoelectronics. In this paper, for the first time to our knowledge, we investigate the characteristics of plasmonic modes in the phosphorene pairs, containing the field enhancement, light confinement, and optical force. The anisotropic dispersion of BP contributes to the direction-dependent symmetric and anti-symmetric plasmonic modes. Our results reveal that the symmetrical modes exhibit stronger field enhancement, higher light confinement, and larger optical force than the anti-symmetric modes in the phosphorene pairs with nanoscale gap distances. The symmetric plasmonic mode along the armchair direction of phosphorene exhibits the light confinement ratio of >90% and optical force of >3000pN/mW. These results would be helpful for the realization of BP-based nanoscale light manipulation and devices.

2. Structure and theoretical analysis

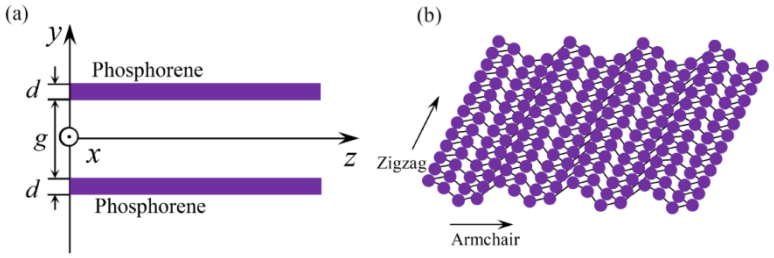

Fig. 1. (a) Schematic diagram of the BP structure consisting of double phosphorene sheets with a gap distance *g*. *d* stands for the thickness of BP layers. Light propagates along the *z*-axis direction. (b) Atomic structure of phosphorene with armchair and zigzag crystal directions.

As shown in Fig. 1, the BP structure is composed of double phosphorene layers (i.e., phosphorene pair) parallel to each other. The gap distance between the BP layers is *g*, the thickness of BP layers is *d*, and the operating wavelength is λ. The optical features of

Optics EXPRESS

phosphorene sheet can be described using the semi-classical Drude model [31, 34]. The direction-dependent conductivities of phosphorene can be expressed as

$$\delta_{jj} = iD_j / [\pi(\omega + i\varsigma/\hbar)], \tag{1}$$

where $D_j = \pi e^2 n/m_j$ is the Drude weight, j represents the x-, y-, and z-axis directions, ω is the angular frequency of light in vacuum, and ς is the electron relaxation rate of BP. n is the electron doping. The electron masses in the x-axis (armchair) and z-axis (zigzag) directions of BP layers can be described as

$$m_{cx} = \hbar^2 / [2\gamma^2/\Delta + \varsigma_c], \quad m_{cz} = \hbar^2 / [2\upsilon_c], \tag{2}$$

where ς_c and υ_c are related to the effective masses, γ describes the effective coupling of band edges, and Δ is the energy band gap. Through fitting the anisotropic mass, the above parameters for the BP layer can be set as $\gamma = 4a/\pi$ eVm, $\Delta = 2$ eV, $\varsigma_c = \hbar^2/0.4m_0$, $\upsilon_c = \hbar^2/1.4m_0$, $n = 10^{13}$ cm^{-2}, and $\varsigma = 10$ meV, respectively [31]. a (≈0.223 nm) stands for the scale length of BP and thus π/a is the width of Brillouin Zone. m_0 is the electron mass, and $\hbar$ is the reduced Planck's constant. The optical parameter of phosphorene can be described employing the equivalent relative permittivity, which depends on the conductivity and can be expressed as

$$\varepsilon_{jj} = \varepsilon_r + \frac{i\delta_{jj}}{\varepsilon_0 \omega d}, \tag{3}$$

where ε_r equals to 5.76 for the BP layer. We can see from above equations that the relative permittivity of the BP depends on the direction (x or z axis) of light propagation, anticipating the anisotropic optical properties. In our calculations, the BP thickness is reasonably set as d = 1 nm [31]. As depicted in Fig. 2(a) and 2(b), the relative permittivities of phosphorene are different in the x- and z-axis directions, which results from the direction-dependent effective mass. The real part of the relative permittivities is less than naught in the infrared region (e.g., λ = 30 μm), which is similar to the property of graphene [24]. Thus, the phosphorene sheets can support and propagate transverse magnetic (TM) plasmonic waves. The dispersion characteristics of plasmonic waves in the BP structures can be achieved from the Maxwell's equations and boundary conditions. Assuming the fields of the light propagation in the phosphorene pairs possess the form of exp($i\beta z$-$i\omega t$), the electric field in the y-axis direction for TM waves can be described as

$$E_y = E_0 \begin{cases} \cos(-\frac{k_y d}{2} + \theta)\Psi(y) & 0 < |y| < \frac{g}{2} \\ \frac{1}{\varepsilon_y}\cos[k_y(|y| - \frac{g}{2} - \frac{d}{2}) + \theta] & \frac{g}{2} < |y| < \frac{g}{2} + d, \\ \cos(\frac{k_y d}{2} + \theta)\exp[-\chi(|y| - \frac{g}{2} - d)] & |y| > \frac{g}{2} + d \end{cases} \tag{4}$$

where $\Psi(y)$ is equal to $\cosh(\chi y)/\cosh(\chi g/2)$ for symmetric mode and to $\sinh(\chi y)/\sinh(\chi g/2)$ for anti-symmetric mode, θ is the phase shift of the field in the middle of the BP waveguide owing to the coupling behavior, and β is the propagation constant of the modes. k_y is the wavevector of light in the BP structure along y-axis direction, and χ is the field decay rate in the space, which are determined by

$$\frac{\beta^2}{\varepsilon_y} + \frac{k_y^2}{\varepsilon_z} = k_0^2, \quad \beta^2 - \chi^2 = k_0^2, \tag{5}$$

Optics EXPRESS

where k_0 is the wavevector of incident light in vacuum. Derived from the Maxwell's equations, the electric field E_z can be described as $E_z = i\varepsilon_y \partial E_y / \beta \varepsilon_z \partial y$. Thus, the detailed form of E_z in the phosphorene pairs can be expressed as

$$E_z = E_0 \begin{cases} \frac{i\chi}{\beta}\cos(-\frac{k_y d}{2}+\theta)\Psi'(y) & 0 < |y| < \frac{g}{2} \\ -\frac{ik_y}{\beta\varepsilon_z}\frac{y}{|y|}\sin[k_y(|y|-\frac{g}{2}-\frac{d}{2})+\theta] & \frac{g}{2} < |y| < \frac{g}{2}+d, \\ -\frac{i\chi}{\beta}\frac{y}{|y|}\cos(\frac{k_y d}{2}+\theta)\exp[-\chi(|y|-\frac{g}{2}-d)] & |y| > \frac{g}{2}+d \end{cases} \quad (6)$$

where $\Psi'(y)$ is expressed as $\sinh(\chi y)/\cosh(\chi g/2)$ for symmetric mode and $\cosh(\chi y)/\sinh(\chi g/2)$ for anti-symmetric mode. Owing to the continuity conditions of tangential component E_z at the interfaces (i.e., $y = \pm g/2$ and $y = \pm (g/2 + d)$), the characteristic equations of fundamental plasmonic modes in the phosphorene pairs can be governed by

$$\tan(-\frac{k_y d}{2}+\theta) = -\frac{\chi\varepsilon_z}{k_y}\Theta, \quad (7)$$

$$\tan(\frac{k_y d}{2}+\theta) = \frac{\chi\varepsilon_z}{k_y}, \quad (8)$$

where $\Theta = \tanh(\chi g/2)$ for symmetric mode, and $\Theta = \coth(\chi g/2)$ for anti-symmetric mode. Thus, the dispersion and field distributions of plasmonic modes can be theoretically obtained by solving above equations. We can see from Figs. 2(c) and 2(d) that the effective refractive indices (n_{eff}) of symmetric plasmonic modes are larger than those of anti-symmetric modes for both the armchair and zigzag directions. When g is fixed, the plasmonic waves along the armchair direction possess larger effective refractive indices than the zigzag direction for both the symmetric and anti-symmetric modes. The theoretical results agree well with the finite element method (FEM) simulations. It is worth noting that n_{eff} decreases with increasing g for symmetric modes, while increases for anti-symmetric modes. The convergence appears for the two modes when g is large enough (e.g., g>180 nm for zigzag direction).

Optics EXPRESS

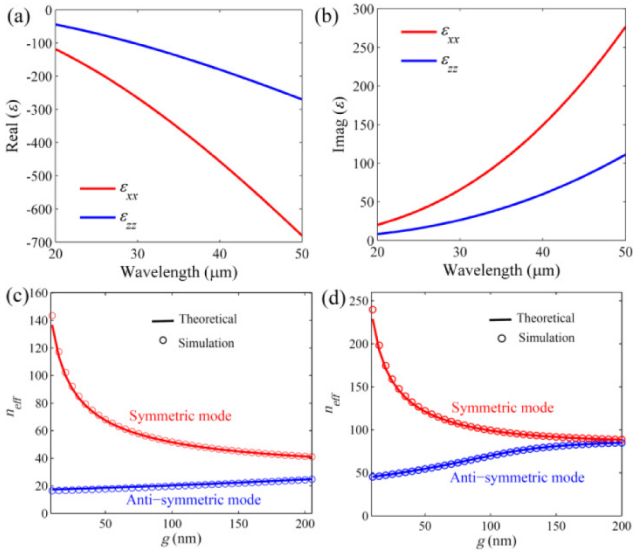

Fig. 2. (a) Real and (b) imaginary parts of the relative permittivities of phosphorene in the *x*-axis (armchair) and *z*-axis (zigzag) directions in the infrared regions. (c)-(d) Effective refractive indices (n_{eff}) of fundamental symmetric and anti-symmetric plasmonic modes with different gap distances *g* at λ = 30 μm when the plasmonic waves propagate along the armchair and zigzag directions.

3. Results and discussion

The electric field enhancement is a crucial factor for the plasmonic waveguides, which can be defined as the ratio of electric field $|E_y|$ at the BP boundaries (i.e., $\eta = |E_y|(y = 2/g)/|E_y|(y = 2/g + d)$). According to Eq. (4), the field enhancement factor can be expressed as

$$\eta = \sqrt{\frac{\chi^2\varepsilon_z^2 + k_y^2}{\chi^2\varepsilon_z^2\Theta^2 + k_y^2}}, \tag{9}$$

where $\Theta = \tanh(\chi g/2)$ for symmetric mode, and $\Theta = \coth(\chi g/2)$ for anti-symmetric mode. We plot the field enhancement factors and electric field distributions of the plasmonic modes in the armchair and zigzag directions, as shown in Fig. 3. The results illustrate that the optical field in the phosphorene pairs can be obviously enhanced for the symmetric modes. It is worth noting that the field enhancement is stronger when the BP layers get closer to each other. However, the anti-symmetric plasmonic modes will not able to generate the field enhancement, and decrease with *g*. The theoretical calculations are in excellent agreement with the FEM simulations. These properties can be easily explained by analyzing the term Θ^2 in Eq. (9). For the symmetric modes, $\Theta^2 = \tanh^2(\chi g/2)$ is less than 1 and monotonously increases with *g* when $g>0$. Thus, η will be larger than 1 and increases with the decrease of *g*. The reverse is the case for the anti-symmetric modes. In addition, the field enhancement factor of symmetric plasmonic modes along the armchair direction in the phosphorene pairs can approach larger than 7 when $g<9$ nm. The amplitudes of E_y between the BP layers are larger than that outside the BP layers for the symmetric modes, while the reverse is the case for the anti-symmetric modes, as can be seen in the insets of Fig. 3.

Optics EXPRESS

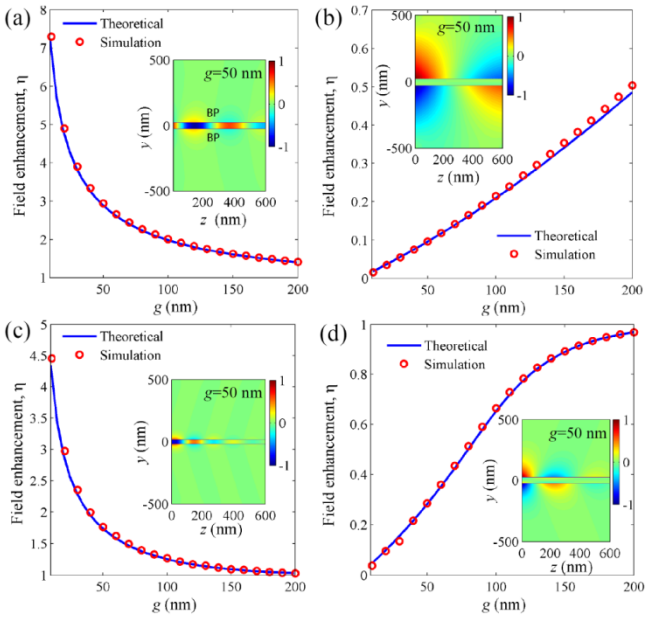

Fig. 3. Field enhancement factors (η) of (a) symmetric and (b) anti-symmetric modes in the phosphorene pairs with different g at λ = 30 μm when the plasmonic mode propagates along the armchair direction. Field enhancement factors of (c) symmetric and (d) anti-symmetric plasmonic modes propagating along the zigzag direction. The insets show the field distributions of E_y in the phosphorene pairs with g = 50 nm.

Subsequently, we investigate the light confinement ratio in the phosphorene pairs, which is defined as the ratio of the integrated Poynting vector P_z in the regions between and outside the BP layers,

$$\xi = \int_{-g/2}^{g/2} P_z ds \Big/ \int_{-\infty}^{\infty} P_z ds. \tag{10}$$

We can obtain the distributions of P_z in the BP structures using the FEM simulations. The light confinement ratio ξ can be calculated by integrating P_z perpendicular to the BP layers. Figure 4 shows the light confinement ratio of the plasmonic modes in the phosphorene pairs. It is found that the light field is strongly confined in the BP layers for the symmetric modes. The light confinement ratio can approach more than 90% in the phosphorene pairs with g<9 nm, which is remarkable compared to the result in hyperbolic metamaterials [35]. The light confinement ratios still possess the ultra-high level of >70% and >50% for the symmetric modes propagating in the armchair and zigzag directions when g = 200 nm, respectively. As shown in the inset of Fig. 4(a), the major light power of symmetrical modes can be concentrated in the region between the BP layers. However, the light confinement ratio of anti-symmetric mode is less than 10% in the BP structure for the plasmonic propagation along the armchair direction. Thus, the light power mainly distributes outside the phosphorene pairs, as depicted in the inset of Fig. 4(b). As shown in Fig. 4(c), the confinement of symmetric plasmonic mode in the zigzag direction is weaker than that of armchair direction. But, the confinement of anti-symmetric plasmonic mode is stronger for the propagation in the zigzag direction, as can be seen in Fig. 4(d).

Optics EXPRESS

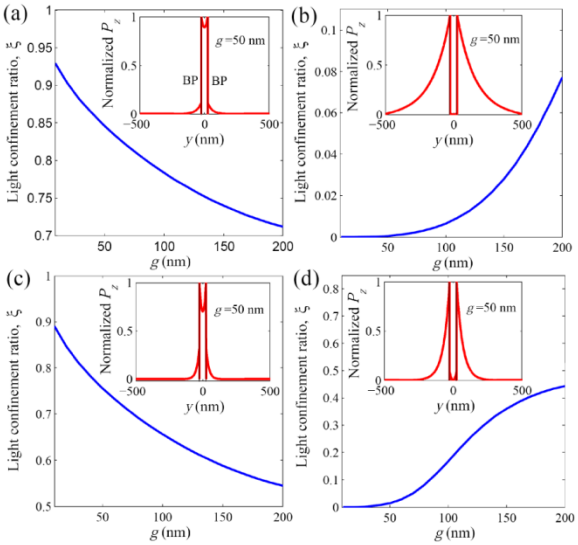

Fig. 4. Light confinement ratios (ζ) of (a) symmetric and (b) anti-symmetric modes in the phosphorene pairs with different g at λ = 30 μm when the plasmonic waves propagate in the armchair direction of BP layers. Light confinement ratios of (c) symmetric and (d) anti-symmetric plasmonic modes propagating in the zigzag direction. The insets show the profiles of P_z perpendicular to the BP layers with g = 50 nm.

The strong confinement of light in the waveguides contributes to the generation of giant optical force [36]. According to the energy conservation law in the waveguides with a gap distance g, the optical gradient force (OGF) can be given by

$$f_n(g) = \frac{1}{c}\frac{\partial n_{eff}}{\partial g}\bigg|_{\lambda} \tag{11}$$

where f_n is the optical force per unit length normalized to the local power with a unit of N/m/W. c is the light speed in vacuum. For lossy waveguides, the light propagates with exponentially decaying power: $P(L) = P(0)\exp(-\alpha L)$ [37]. The propagation loss will influence the optical force generated on the waveguides, which can be defined as $L_m = \alpha^{-1} = \lambda/4\pi\mathrm{Im}(n_{eff})$. Thus, the total optical force per unit light power impinging in the phosphorene pair with a length L can be obtained by $F_n = f_n L_m[1-\exp(-L/L_m)]$. Here, L = 500 nm and λ = 30 μm are assumed to theoretically calculate the optical force. The results in Fig. 5 show that the optical force is strongest for the symmetric plasmonic mode in the armchair direction, which could reach over 3000 pN/mW when g<9 nm. The optical force is still larger than 320 pN/mW for the plasmonic modes in the armchair direction when g = 50 nm. This value is excellent when compared to the metal-based plasmonic waveguides [38]. It is worth noting that the symmetric modes possess much stronger optical force than the anti-symmetric modes in the phosphorene pairs with g<90 nm, which can be attributed to the higher optical field intensity between the BP layers for the symmetric modes [36]. As the gap of BP layers decreases, the optical force significantly increases for the symmetric modes. To verify the theoretical results, we calculate the optical force employing the Maxwell's stress tensor (MST) method. The optical force can be obtained using the integration of the MST around the arbitrary surface enclosing the waveguides [38]. The stress tensor is defined as $T_{jk} = \mu_0(H_jH_k - \delta_{jk}H^2/2) + \varepsilon_0(E_jE_k - \delta_{jk}E^2/2)$, where δ stands for the Kronecker delta function. Similar to j, k also denotes the x-, y-, and z-axis directions. The electric and magnetic field distributions are obtained by the FEM simulations. The optical force in the y-axis direction can be described as

Optics EXPRESS

$$F_n = \oint_s \langle T \rangle \cdot e_y ds \tag{12}$$

where s is the arbitrary surface enclosing one phosphorene sheet, and e_y is the unit vector in the y-axis direction. The incident power $P(0) = 1$ W is set to simulate the field distributions of plasmonic modes in the phosphorene pairs. As shown in Fig. 5, the results obtained by the MST method are in good agreement with the theoretical calculations. In the calculations, the BP layers are considered as the uniform planes [31]. If there exists a ununiformity (e.g., 1 nm) between the BP layers, the relative deviations of field enhancement, light confinement, and optical force we calculated for the symmetric plasmonic modes in armchair direction are less than 6%, 1%, and 10% when g>10 nm, respectively.

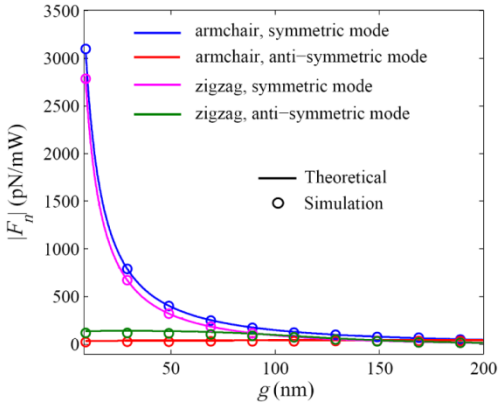

Fig. 5. Optical forces between the phosphorene pairs with L = 500 nm and $P(0)$ = 1 W for the symmetric and anti-symmetric plasmonic modes along the armchair and zigzag directions. The operating wavelength is 30 μm. The curves and circles denote the theoretical and simulation results obtained by the OGF and MST methods, respectively.

4. Conclusions

In this paper, we have theoretically and numerically investigated the responses of field enhancement, light confinement, and optical force of plasmonic modes in phosphorene pairs. We have found that the plasmonic modes are particularly dependent on the propagation direction due to the anisotropic dispersion of BP. The results illustrate that the symmetric plasmonic modes exhibit the stronger field enhancement, higher light confinement, and larger optical force than the anti-symmetric modes in the phosphorene pairs with nanoscale gap distances. The field enhancement and optical force for the symmetric modes can be enlarged by decreasing the gap distance. The light confinement ratio can exceed 90% for the symmetric plasmonic mode along the armchair direction of BP layers. The optical force can approach over 3000 pN/mW in the phosphorene pair with a length of only 500 nm, which is excellent compared to the metal-based plasmonic systems. The theoretical calculations are consistent with the FEM simulations. These results could pave a pathway toward the BP-based light manipulation and optical functional devices.

Funding

This work was supported by the National Natural Science Foundation of China (11634010, 61575162, and 61377035) and Fundamental Research Funds for the Central Universities (3102016OQD031 and G2016KY0303).

Acknowledgments

The authors would like to thank Dr. Qingliang Feng for the useful discussion.

193.03.141.93 {ts '2018-01-05 03:27:32'}